Application of the Continuous Stern-Gerlach Effect for Laser Spectroscopy of the $^{40}Ar^{13+}$ Fine Structure in a Penning Trap

Alexander Egl,[1,*] Ioanna Arapoglou,[1] Martin Höcker,[1] Kristian König,[2] Tim Ratajczyk,[2] Tim Sailer,[1] Bingsheng Tu,[1] Andreas Weigel,[1] Klaus Blaum,[1] Wilfried Nörtershäuser,[2] and Sven Sturm[1]

[1]*Max-Planck-Institut für Kernphysik, Saupfercheckweg 1, 69117 Heidelberg, Germany*

[2]*Institut für Kernphysik, Technische Universität Darmstadt, 64289 Darmstadt, Germany*

(Received 2 May 2019; revised manuscript received 5 July 2019; published 20 September 2019)

We report on the successful demonstration of a novel scheme for detecting optical transitions in highly charged ions. We applied it to determine the frequency of the dipole-forbidden $2p\,^2P_{1/2} - {}^2P_{3/2}$ transition in the fine structure of $^{40}Ar^{13+}$ using a single ion stored in the harmonic potential of a Penning trap. Our measurement scheme does not require detection of fluorescence, instead it makes use of the continuous Stern-Gerlach effect. Our value of $679.216464(4)_{\mathrm{stat}}(5)_{\mathrm{syst}}$ THz is in reasonable agreement with the current best literature values and improves its uncertainty by a factor of 24.

DOI: 10.1103/PhysRevLett.123.123001

Highly charged ions (HCI) are model systems for many different physics disciplines and enable very important and unique tests of fundamental theories. Because of the compression of the orbitals with high nuclear charge Z, the electrons in HCI are localized close to the nucleus and experience very strong electromagnetic fields. Hence they are predestined for testing bound-state quantum electrodynamics calculations in extreme conditions as well as relativistic many-body interactions and nuclear effects. As a further consequence of these immense field strengths, many well-known effects are occurring at different energy scales compared to atoms or singly charged ions. Depending on the nuclear charge Z and electronic charge state of the HCI, principal transitions can be shifted to the keV range and fine structure or hyperfine structure transitions become accessible for laser spectroscopy [1–9].

For the production of such ions, ionization energies which can range from hundreds of eV up to 100 keV for hydrogenlike lead have to be reached. The commonly used tools to produce and store such high charge states are electron-beam ion traps (EBIT) [10] or storage rings coupled to accelerator facilities [11]. These devices, however, typically feature conditions that hinder reaching high spectroscopic precision, such as high temperatures in the case of an EBIT [9,12,13] and high kinetic energies in storage rings [1–7]. Hence, in both cases activities are going on to extract ions from the production environment [14,15], cool them, and perform high-resolution laser spectroscopy. While in some cases traditional fluorescence spectroscopy can be employed [16–18], in most cases the electric-dipole forbidden transitions have long lifetimes and consequently prohibitively low photon yields. Whereas these systems provide excellent conditions for many applications, for instance, usage as a frequency standard, they require more sophisticated detection schemes, such as, e.g., quantum logic spectroscopy [19,20].

In this Letter we present a novel technique that enables an efficient search for such narrow transitions as well as the precise spectroscopy of the respective long-lived states. For our demonstration experiment, we store a single $^{40}Ar^{13+}$ ion in the cryogenic Penning-trap system of the ALPHATRAP experiment. Making use of the continuous Stern-Gerlach effect, ALPHATRAP can unambiguously determine the magnetic moment projection of the ion. This way, virtually every successful excitation of the ion by optical or microwave photons that alters the magnetic substate can be detected. By finding and measuring the optical fine structure transition frequency in the boronlike argon ion we show—to our knowledge for the first time—the experimental realization of this technique. In the current conception, as a proof of principle, the achieved precision of this transition frequency is mainly limited by the first-order Doppler width of the trapped ion at about 1 K. Lowering the ion temperature by means of sympathetic laser cooling [21] or resolving individual motional sidebands [22] should allow for spectroscopy close to the natural linewidth.

At ALPHATRAP the HCI are produced externally in dedicated ion sources, like the cryogenic HD-EBIT [10] or a Heidelberg compact HC-EBIT [23], from which the HCI can be extracted, transported, and injected via an ultrahigh vacuum beam line into the double Penning-trap system. The Penning trap allows us to manipulate and spatially confine a single charged particle at low energies. By a superposition of static electric and magnetic fields the ion is forced onto a trajectory which is the superposition of three independent eigenmotions with respective eigenfrequencies (ν_i), namely, in the radial plane the modified

cyclotron motion (ν_+) and the magnetron motion (ν_-). Perpendicular to those the axial motion (ν_z), which is parallel to the magnetic field and laser light direction. These frequencies follow the hierarchy $\nu_+ \gg \nu_z \gg \nu_-$ [24] and can be combined as $\nu_c^2 = \nu_+^2 + \nu_z^2 + \nu_-^2$ to yield the free cyclotron frequency $\nu_c = (1/2\pi)(q_{\mathrm{ion}}/m_{\mathrm{ion}})B_0$ [25], which in turn depends solely on the magnetic field B_0, the mass m_{ion}, and charge q_{ion} of the ion. This field can be measured to a sufficient precision [21] to correct the transition frequency for the Zeeman shift. The double-trap system consists of a precision trap (PT) and an analysis trap (AT) inserted into a superconducting magnet with a homogeneous field B_0^{PT} of 4.02 T at the center of the PT. For the determination of the ion's axial frequency, both in the PT and AT, a tuned superconducting tank circuit is connected to one of the electrodes. This allows us to measure the image currents induced by the motion of the ion and to convert them to a voltage which is subsequently amplified by a cryogenic low-noise amplifier [21,26]. The ion dissipates its energy into the tank circuit, which is cooled by the cryostat to a temperature of liquid helium of typically 4.2 K. In thermal equilibrium the ion's motion cancels the thermal Johnson noise of the tank circuit at the frequency of the motion. This bolometric type of detection [27,28] cools the ion to the electron gas temperature of the resonator with a cooling time constant τ_z of typically few tens of ms.

For cooling also the modified cyclotron and magnetron mode, sideband coupling techniques can be used [25,29]. By applying a quadrupolar excitation of frequency ν_{rf} and with suitable geometry the axial and radial modes can be coupled. This coupling will exchange action between the modes and while the axial mode is kept in thermal contact with the resonator, also the radial modes will be cooled resistively to a thermal equilibrium (Boltzmann) distribution to which a temperature $T_\pm$ can be assigned:

$$\langle E_\pm \rangle = k_B T_\pm = \pm k_B \frac{\nu_\pm}{\nu_z} T_z, \tag{1}$$

with $E_\pm$ being the energy in the respective mode and k_B the Boltzmann constant. A further reduction in the ion's energy can be accomplished by feeding the detected thermal noise with suitable amplitude and phase back to the tank circuit [30,31]. Depending on the signal-to-noise ratio of the cryogenic amplifier, the temperature can be reduced by a factor of ≈ 5.

For probing the fine structure transition the ion is transported to the PT, whereas the readout and preparation of the spin state is done in the AT. In the AT, the central ring electrode is made of a ferromagnetic cobalt-iron alloy and the homogeneous magnetic field gets modified to an inhomogeneous magnetic bottle of shape: $B^{\mathrm{AT}}(z) = B_0^{\mathrm{AT}} + B_2^{\mathrm{AT}} z^2$, where z is the coordinate in the axial direction. In our case the B_2^{AT} term amounts to around 44 $\mathrm{kT/m^2}$. This magnetic bottle

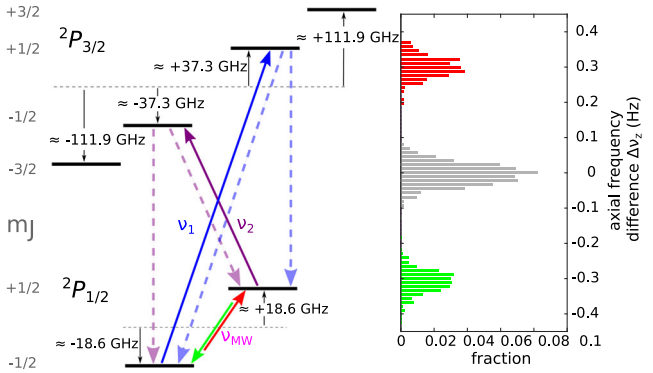

FIG. 1. (Left) Level scheme for $^{40}Ar^{13+}$ in which the strong magnetic field B_0^{PT} lifts the degeneracy of the Zeeman levels. The transition frequency $\nu_{1,2}$ between $^2P_{1/2}$ and $^2P_{3/2}$ is about 679 THz, which corresponds to a wavelength of 441 nm. The two investigated transition cycles are shown in purple and blue; solid lines indicate the transitions driven by the laser and the dotted lines the possible channels for spontaneous decay. (right) Axial frequency difference $\Delta\nu_z$ in ν_z^{AT} for subsequent measurements after microwave irradiation. For 0 Hz no spin state transition happened, whereas a change of ± 0.3 Hz indicates a transition between the $|1/2, \pm 1/2\rangle$ states, corresponding to the transitions indicated by the green and red arrows on the left-hand side.

maps the magnetic moment and thus the spin state of the electron to the ion's motional state, a method referred to as the continuous Stern-Gerlach effect. Depending on the orientation of the spin state of the electron the ion experiences a shift $\Delta\nu_z$ in the axial frequency ν_z^{AT} given by [32]

$$\Delta\nu_z \approx \pm \frac{g_J \mu_B B_2^{\mathrm{AT}}}{8\pi^2 m_{\mathrm{ion}} \nu_z^{\mathrm{AT}}}, \tag{2}$$

where g_J is the bound electron g factor for the $J = 1/2$ ground state [33] and μ_B the Bohr magneton.

In our case we performed laser spectroscopy on the 441 nm fine structure transition between the $2p\,^2P_{1/2}$ and $^2P_{3/2}$ state in boronlike argon. To this end a single $^{40}Ar^{13+}$ ion was trapped in the cryogenic cylindrical Penning-trap system [21]. For $^{40}Ar^{13+}$ in the $^2P_{1/2}$ ground state, the nominal axial frequency difference between the spin-up $|J, m_J\rangle = |1/2, +1/2\rangle$ and the spin-down state $|1/2, -1/2\rangle$ amounts to 309 mHz at an axial frequency ν_z^{AT} of 334 kHz, which can be measured in a nondestructive way; see Fig. 1.

For production of the laser light at 441 nm a diode-pumped solid-state laser (Coherent Verdi V18) at 532 nm is pumping a titanium:sapphire crystal in a ring laser cavity (Sirah Matisse 2TS) which can be locked to a fiber-coupled reference cavity for stabilization. The output of the ring laser at 882 nm is then frequency doubled by a stand-alone ring cavity (Spectra-Physics Wavetrain 2). For frequency stabilization a wavelength meter (High Finesse WS-Ultimate 2) with a specified accuracy of 2 MHz and a resolution of

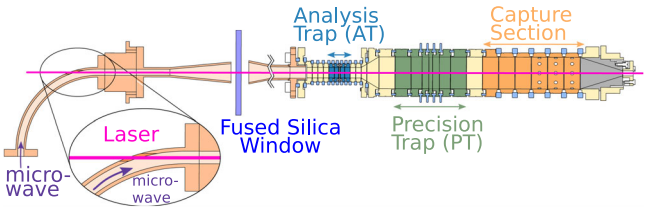

FIG. 2. Schematics (not to scale) of the combined microwave and laser in-coupling. The laser beam is depicted as a magenta line and the propagation path of the microwave in a waveguide structure is indicated by a purple arrow. The trap tower consist of the analysis trap (blue), the precision trap (green) and capture section (orange) for capturing and storing externally injected HCI. Compartments of the double-stage cryostat at different vacuum pressures and temperatures are separated by quartz glass windows and traversed by microwave horn antennas facing each other [21].

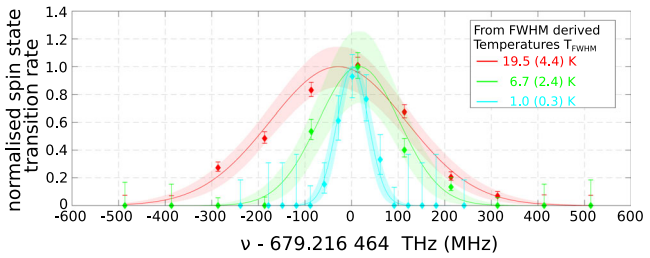

FIG. 3. Typical resonances measured for different axial temperatures. The resonance in red is taken without any further cooling, whereas the green, respectively, cyan one were taken using adiabatic cooling only or, respectively, in addition to negative feedback cooling. The error bars are the maximum likelihood estimates for binomial attempts for obtaining a spin state transition at the respective frequency. The solid curve is a Gaussian line shape fitted with a maximum-likelihood fit routine. The shaded area shows the confidence band (68% level) of the fit. The datasets shown here correspond to measurement numbers 8, 9, and 12 in Fig. 4.

200 kHz is used. The wavelength meter is calibrated in regular intervals by an iodine-stabilized helium-neon laser (Lasertex LJCS-3-11) with a relative frequency repeatability of 2.5×10^{-11}. At the beginning and the end of the measurement campaign, stretching over five months, the absolute calibration of the wavelength meter by the helium-neon laser was compared against a GPS-referenced frequency comb (Menlo Systems FC1500-250-WG) located at the Institut für Kernphysik in Darmstadt. For this purpose the wavelength meter and the helium-neon laser were transported between the two sites. These calibrations were in agreement, confirming an absolute frequency repeatability better than 2.6 MHz at 882 nm. Adjusting the piezo actuators in the reference cavity of the Ti:sapphire ring laser allows us to stabilize the second harmonic frequency in the long term to a stability better than 1 MHz using the error signal derived from the wavelength meter. The beam is guided in a single-mode optical fiber to a breadboard with the in-coupling optics mounted below the magnet bore, where it is axially overlapped with the microwave; see Fig. 2.

The microwave in turn is used to induce transitions in the $|1/2, \mp 1/2\rangle$ ground state levels (see Fig. 1) for the spin state analysis and a deterministic preparation in either the $|1/2, -1/2\rangle$ or $|1/2, +1/2\rangle$ state in the AT. The ion can be transported adiabatically between the AT and PT, with negligible heating of the ion motions [21]. Furthermore, spontaneous radiative decay of the magnetic substate occurs only on a timescale of years [34].

Upon initialization in one of the two $|1/2, \mp 1/2\rangle$ states, the ion is transported to the PT where it is irradiated with a collimated laser beam with a Gaussian beam profile and a diameter of 2 mm for typically 30 s in order to excite the transition ν_1 or ν_2 to the corresponding $|3/2, \pm 1/2\rangle$ state (see Fig. 1). The lifetime of the excited state $^2P_{3/2}$ is around 9.6 ms [35,36]. The spontaneous decay will be preferably projection conserving. After continuous resonant excitation the ion is eventually pumped into the other magnetic substate. Because of the strong Zeeman shifts, this final state is far off resonant and therefore a dark state. After probing the ion by the laser, it is shuttled back to the AT where the spin state is analyzed and subsequently reinitialized into the initial m_J spin state. By repeating this procedure multiple times at different probe frequencies of the laser in a randomized order allows to deduce a frequency dependent spin state transition probability and a resonance can be sampled, as shown in Fig. 3. The measurement time for such cycles is typically around 5 min and the acquistion time for one resonance 24 to 48 h. The laser line width is typically less than 100 $\mathrm{kHz_{rms}}/100$ ms and the laser intensity at the position of the ion was varied between 20 and 50 $\mu\mathrm{W\,mm^{-2}}$ without adjusting the polarization after outcoupling of the optical fiber.

Because the natural line width $\Delta\nu$ of the transition is much smaller than the axial frequency ν_z^{PT} of 650 kHz and due to the harmonic motion of the ion at discrete frequencies, it gives rise to a discrete structure of sidebands [37,38] of width $\Delta\nu$, equally spaced by ν_z^{PT} around the carrier transition frequency. Because of technical limitations in the current setup, those sidebands are not resolvable. Otherwise, the determination of the carrier frequency of the sideband spectrum down to the natural line width should be possible. Sidebands of the radial modes [22] are not observed because the wave vector of the laser beam is ideally purely oriented along the axial direction of ion motion. The final expected line shape can be calculated by a summation of all sideband spectra for a given particle temperature [39]. The full width at half maximum (FWHM) δf of the envelope equals the width one obtains by using the well-known formula for the Doppler broadening in an ideal gas, $\delta f = \sqrt{8 k_B T_z \ln(2)/m_{\mathrm{ion}} c^2}\,\nu_0$, where c is the speed of light and ν_0 the transition frequency of the ion at rest. We can narrow the width of the resonance by either

TABLE I. Relative contribution of individual effects on the systematic error for the determination of the transition frequency. The calibration of the laser frequency is the dominant source of uncertainty. "abs." denotes absolute.

Laser frequency determination (abs.)	$<7.7\times10^{-9}$
B-field stability (abs.)	$<4\times10^{-11}$
Second-order Doppler shift	$<5\times10^{-14}$
Residual B_2^{PT}	$<3\times10^{-15}$
Total	$\leq 7.7\times10^{-9}$

cooling the ion with negative electronic feedback or by decreasing the trapping potential depth adiabatically by a factor ξ. The latter leads to a reduced kinetic energy $\langle E_z\rangle = k_B T_z$ and thus the ion's temperature by $\sqrt{\xi}$. Furthermore, we also showed that both techniques can be combined, which allowed measuring the narrowest resonance, see Fig. 3.

As a consistency check measurements of resonances at different ion temperatures respectively energies were performed. Because of intermittent technical problems in the detection electronics during the data acquisition, the temperature of the ion was elevated by increased and temporally variable electronic noise. This was confirmed by independent measurement methods [40] indicating an axial resonator temperature of 12 to 20 K. Even though this leads to a broadening of the resonance, it is not shifting the center to first order, since the variation of noise level and the selection of probe frequencies was randomly distributed and uncorrelated to the randomized probe frequencies. As shown in Table I, systematic shifts of the resonance center due to an elevated temperature would occur at a level below the measured uncertainty. In order to avoid systematic effects by other parasitically co-trapped ions, we reloaded a second single $^{40}Ar^{13+}$ for the last three measurements replacing the one previously used. Over a total period of two months, in total 13 resonances were recorded with different settings to exclude systematic effects such as power dependencies of the resonance center; see Fig. 4. This time span also corresponds to the storage time of the first ion, indicating vacuum conditions of better than 10^{-17} mbar [21]. The centers of the resonances taken without negative feedback (shown in red in Figs. 3 and 4) seem to be at lower frequencies, however this is statistically nonsignificant and we do not assume this to be due to the temperature of the ion during the measurement but rather a statistical effect. Each single value does not deviate by more than 1.8σ from the weighted mean. Especially the measurements taken by using adiabatic cooling only (9 and 11 in Fig. 4), during which the ion is fully decoupled from the resonator and supposedly most unperturbed, are in good agreement with the weighted mean of all resonances. Estimated contributions to the systematic uncertainties are summarized in Table I.

When combining the results of the individual resonances a value of $679.272651(7)_{\mathrm{stat}}(5)_{\mathrm{syst}}$ THz, and,

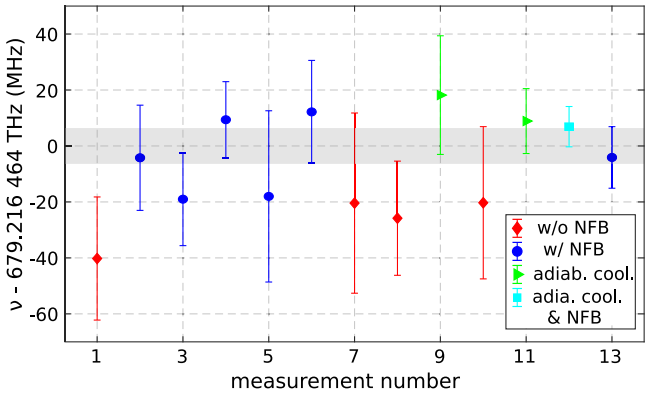

FIG. 4. Centers of resonances taken with different sets of parameters with respect to laser power, laser irradiation time, with or without negative feedback applied or adiabatically cooled. Measurements 1–9 correspond to transition ν_1 whereas measurements 10–13 are taken with transition ν_2 (see Fig. 1). In both cases the center frequencies are corrected for the magnet field including the second-order Zeeman shift. The gray area represents the combined statistical and systematic error.

$679.160272(5)_{\mathrm{stat}}(5)_{\mathrm{syst}}$ THz for the $|1/2,-1/2\rangle \rightarrow |3/2,+1/2\rangle$, respectively, $|1/2,+1/2\rangle \rightarrow |3/2,-1/2\rangle$ transitions in our magnetic field of 4.02 T can be derived. This strong homogeneous magnetic field B_0^{PT} leads to non-negligible contributions by the quadratic Zeeman effect [16] of 2 MHz, which needs to be taken into account, in order to yield the final result of $679.216464(4)_{\mathrm{stat}}(5)_{\mathrm{syst}}$ THz for the $2p\,^2P_{1/2} - {}^2P_{3/2}$ transition. The systematic uncertainty is dominated by the limited resolution of the wavelength meter and the absolute frequency calibration. Having measured these two transition frequencies in a strong magnetic field constitutes also a measurement of the g factor g_J for the excited $J = 3/2$ state. Both the ground state g factor $g_{1/2}$ [33] and the magnetic field B_0^{PT} are known sufficiently well enough, so that a value of 1.33214(15) for $g_{3/2}$ can be derived in agreement with theory [41].

In summary, the M1 fine structure transition $2p\,^2P_{1/2} - {}^2P_{3/2}$ in $^{40}Ar^{13+}$ has been determined to a fractional uncertainty of 9.4×10^{-9}. This result improves previous best measurements by more than an order of magnitude [9,12,13] and is in good agreement with the four results reported in Refs. [9,12] and theoretical calculations [42]. However our value deviates by $3.2\text{-}\sigma$ to lower frequency from Ref. [13], which solely makes up the current value of the NIST database [43]. Taking the weighted mean of all five values published in Refs. [9,12,13] does not show a deviation from our value with a statistical significance.

The applied novel technique relies on a pumping mechanism into a dark state with different spin state configuration, which can be detected by using the continuous Stern-Gerlach effect. This allows us to sweep a large frequency range in order to find a transition which is not *a priori* known to sufficient precision. In multielectron

HCI, where dissimilar electronic configurations can have nearly degenerate (optical) energies, strongly forbidden transitions can be found that feature a strongly suppressed sensitivity to external perturbations or that have strongly enhanced sensitivity to fundamental constants such as the fine structure constant α_{em} [44]. The versatility of our method, combined with the possibility to store and cool arbitrary HCI in ALPHATRAP for virtually indefinite time spans, can be used to search very efficiently for such transitions. Once the transition frequency is determined, the values could serve other experiments [19] as starting points or could also be determined with similar precision directly at ALPHATRAP when the first order Doppler shift is eliminated using the envisaged implementation of sympathetic laser cooling of the HCI [21]. For example, the measurement of rovibrational transitions in H_2^+ gives access to fundamental constants and could pave the way towards a *CPT* test by comparing such transitions to the antimatter equivalent $\bar{H}_2^-$ [45]. Furthermore, a determination of the hyperfine splitting in hydrogen- or lithiumlike bismuth $^{209}Bi^{82+,80+}$, enables a unique test of bound-state QED in the extremely strong magnetic field of the nucleus [46]. From such transitions only a low fluorescence yield can be expected and for long-wavelength transitions, low-noise single-photon detection is not available.

We would like to thank Janko Nauta and Jan-Hendrik Oelmann for their support and P. O. Schmidt and J. R. C. López-Urrutia for discussions. This work was supported by the Max Planck Society (MPG), the International Max Planck Research School for Quantum Dynamics in Physics, Chemistry and Biology (IMPRS-QD), the MPG-PTB-RIKEN Centre for Time, Constants and Fundamental Symmetries, the German Research Foundation (DFG) Collaborative Research Centre "SFB 1225 (ISOQUANT)" and the Helmholtz International Center for FAIR (HIC4FAIR). This Letter comprises parts of the Ph.D. thesis work of A. E. and T. S., to be submitted to Heidelberg University, Germany.

*Corresponding author.
alexander.egl@mpi-hd.mpg.de

[1] I. Klaft, S. Borneis, T. Engel, B. Fricke, R. Grieser, G. Huber, T. Kühl, D. Marx, R. Neumann, S. Schröder *et al.*, Phys. Rev. Lett. **73**, 2425 (1994).
[2] P. Seelig, S. Borneis, A. Dax, T. Engel, S. Faber, M. Gerlach, C. Holbrow, G. Huber, T. Kühl, D. Marx *et al.*, Phys. Rev. Lett. **81**, 4824 (1998).
[3] M. Lochmann, R. Jöhren, C. Geppert, Z. Andelkovic, D. Anielski, B. Botermann, M. Bussmann, A. Dax, N. Frömmgen, M. Hammen *et al.*, Phys. Rev. A **90**, 030501 (R) (2014).
[4] J. Ullmann, Z. Andelkovic, C. Brandau, A. Dax, W. Geithner, C. Geppert, C. Gorges, M. Hammen, V. Hannen, S. Kaufmann *et al.*, Nat. Commun. **8**, 15484 (2017).
[5] M. Vogel and W. Quint, J. Phys. B **42**, 154016 (2009).
[6] J. Ullmann, Z. Andelkovic, A. Dax, W. Geithner, C. Geppert, C. Gorges, M. Hammen, V. Hannen, S. Kaufmann, K. König *et al.*, J. Phys. B **48**, 144022 (2015).
[7] R. Sánchez, M. Lochmann, R. Jöhren, Z. Andelkovic, D. Anielski, B. Botermann, M. Bussmann, A. Dax, N. Frömmgen, C. Geppert *et al.*, J. Phys. B **50**, 085004 (2017).
[8] W. Quint, D. L. Moskovkhin, V. M. Shabaev, and M. Vogel, Phys. Rev. A **78**, 032517 (2008).
[9] V. Mäckel, R. Klawitter, G. Brenner, J. R. Crespo López-Urrutia, and J. Ullrich, Phys. Rev. Lett. **107**, 143002 (2011).
[10] A. J. González Martínez, J. R. Crespo López-Urrutia, D. Fischer, R. Soria Orts, and J. Ullrich, J. Phys. Conf. Ser. **72**, 012001 (2007).
[11] B. Franzke, Nucl. Instrum. Methods B **24–25**, 18 (1987).
[12] I. Draganić, J. R. Crespo López-Urrutia, R. DuBois, S. Fritzsche, V. M. Shabaev, R. S. Orts, I. I. Tupitsyn, Y. Zou, and J. Ullrich, Phys. Rev. Lett. **91**, 183001 (2003).
[13] R. Soria Orts, Z. Harman, J. R. Crespo López-Urrutia, A. N. Artemyev, H. Bruhns, A. J. González Martínez, U. D. Jentschura, C. H. Keitel, A. Lapierre, V. Mironov, V. M. Shabaev, H. Tawara, I. I. Tupitsyn, J. Ullrich, and A. V. Volotka, Phys. Rev. Lett. **97**, 103002 (2006).
[14] H.-J. Kluge, T. Beier, K. Blaum, L. Dahl, S. Eliseev, F. Herfurth, B. Hofmann, O. Kester, S. Koszudowski, C. Kozhuharov *et al.*, Adv. Quantum Chem. **53**, 83 (2008).
[15] L. Schmöger, O. Versolato, M. Schwarz, M. Kohnen, A. Windberger, B. Piest, S. Feuchtenbeiner, J. Pedregosa-Gutierrez, T. Leopold, P. Micke *et al.*, Science **347**, 1233 (2015).
[16] D. von Lindenfels, M. Wiesel, D. A. Glazov, A. V. Volotka, M. M. Sokolov, V. M. Shabaev, G. Plunien, W. Quint, G. Birkl, A. Martin, and M. Vogel, Phys. Rev. A **87**, 023412 (2013).
[17] Z. Andelkovic, R. Cazan, W. Nörtershäuser, S. Bharadia, D. M. Segal, R. C. Thompson, R. Jöhren, J. Vollbrecht, V. Hannen, and M. Vogel, Phys. Rev. A **87**, 033423 (2013).
[18] T. Murböck, S. Schmidt, G. Birkl, W. Nörtershäuser, R. C. Thompson, and M. Vogel, Phys. Rev. A **94**, 043410 (2016).
[19] P. O. Schmidt, T. Rosenband, C. Langer, W. M. Itano, J. C. Bergquist, and D. J. Wineland, Science **309**, 749 (2005).
[20] T. Leopold, S. A. King, P. Micke, A. Bautista-Salvador, J. C. Heip, C. Ospelkaus, J. R. Crespo López-Urrutia, and P. O. Schmidt, Rev. Sci. Instrum. **90**, 073201 (2019).
[21] S. Sturm, I. Arapoglou, A. Egl, M. Höcker, S. Kraemer, T. Sailer, B. Tu, A. Weigel, R. Wolf, J. R. Crespo López-Urrutia, and K. Blaum, Eur. Phys. J. Spec. Top. **227**, 1425 (2019).
[22] S. Mavadia, G. Stutter, J. F. Goodwin, D. R. Crick, R. C. Thompson, and D. M. Segal, Phys. Rev. A **89**, 032502 (2014).
[23] P. Micke, S. Kühn, L. Buchauer, J. Harries, T. M. Bücking, K. Blaum, A. Cieluch, A. Egl, D. Hollain, S. Kraemer *et al.*, Rev. Sci. Instrum. **89**, 063109 (2018).
[24] F. G. Major, V. N. Gheorghe, and G. Werth, *Charged Particle Traps: Physics and Techniques of Charged Particle Field Confinement* (Springer Science & Business Media, Berlin Heidelberg, 2006), Vol. 37.

[25] L. S. Brown and G. Gabrielse, Rev. Mod. Phys. **58**, 233 (1986).
[26] A. Weigel, Ph.D. thesis, Ruprecht-Karls Universität Heidelberg, 2019.
[27] H. Dehmelt and F. Walls, Phys. Rev. Lett. **21**, 127 (1968).
[28] D. Wineland and H. Dehmelt, J. Appl. Phys. **46**, 919 (1975).
[29] E. A. Cornell, R. M. Weisskoff, K. R. Boyce, and D. E. Pritchard, Phys. Rev. A **41**, 312 (1990).
[30] H. Dehmelt, W. Nagourney, and J. Sandberg, Proc. Natl. Acad. Sci. U.S.A. **83**, 5761 (1986).
[31] B. D'Urso, B. Odom, and G. Gabrielse, Phys. Rev. Lett. **90**, 043001 (2003).
[32] F. Köhler-Langes, *The Electron Mass and Calcium Isotope Shifts* (Springer International Publishing, Switzerland, 2017).
[33] I. Arapoglou, A. Egl, M. Höcker, T. Sailer, B. Tu, A. Weigel, R. Wolf, H. Cakir, V. A. Yerokhin, N. S. Oreshkina, V. A. Agababaev, A. V. Volotka, D. V. Zinenko, D. A. Glazov, Z. Harman, C. H. Keitel, S. Sturm, and K. Blaum, Phys. Rev. Lett. **122**, 253001 (2019).
[34] W. Quint and M. Vogel, *Fundamental Physics in Particle Traps* (Springer, New York, 2014), Vol. 395.
[35] A. Lapierre, U. D. Jentschura, J. R. Crespo López-Urrutia, J. Braun, G. Brenner, H. Bruhns, D. Fischer, A. J. González Martínez, Z. Harman, W. R. Johnson, C. Keitel, V. Mironov, C. J. Osborne, G. Sikler, R. Soria Orts, V. M. Shabaev, H. Tawara, I. I. Tupitsyn, J. Ullrich, and A. V. Volotka, Phys. Rev. Lett. **95**, 183001 (2005).
[36] A. Lapierre, J. R. Crespo López-Urrutia, J. Braun, G. Brenner, H. Bruhns, D. Fischer, A. J. González Martínez, V. Mironov, C. Osborne, G. Sikler, R. Soria Orts, H. Tawara, J. Ullrich, V. M. Shabaev, I. I. Tupitsyn, and A. Volotka, Phys. Rev. A **73**, 052507 (2006).
[37] R. Dicke, Phys. Rev. **89**, 472 (1953).
[38] D. J. Wineland and W. M. Itano, Phys. Rev. A **20**, 1521 (1979).
[39] The single ion interacting with the resonator that acts as a thermal heat bath can be considered an ergodic system. Back to back measurements of the temperature over a period much longer than the cooling time constant τ_z resembles the thermal Boltzmann distribution with the equilibrium temperature between ion and the thermal heat bath.
[40] S. Djekic, J. Alonso, H.-J. Kluge, W. Quint, S. Stahl, T. Valenzuela, J. Verdú, M. Vogel, and G. Werth, Eur. Phys. J. D **31**, 451 (2004).
[41] V. Agababaev, D. Glazov, A. Volotka, D. Zinenko, V. M. Shabaev, and G. Plunien, X-Ray Spectrom., https://doi.org/10.1002/xrs.3074.
[42] A. N. Artemyev, V. M. Shabaev, I. I. Tupitsyn, G. Plunien, A. Surzhykov, and S. Fritzsche, Phys. Rev. A **88**, 032518 (2013).
[43] A. Kramida, Yu. Ralchenko, and J. Reader (NIST ASD Team), NIST Atomic Spectra Database (ver. 5.6.1), National Institute of Standards and Technology, Gaithersburg, MD, 2018, https://physics.nist.gov/asd.
[44] M. G. Kozlov, M. S. Safronova, J. R. Crespo López-Urrutia, and P. O. Schmidt, Rev. Mod. Phys. **90**, 045005 (2018).
[45] E. G. Myers, Phys. Rev. A **98**, 010101(R) (2018).
[46] M. Vogel and W. Quint, Hyperfine Interact. **196**, 93 (2010).